Translational Oncology 62 (2025) 102535

Contents lists available at ScienceDirect

Translational Oncology

journal homepage: www.elsevier.com/locate/tranon

Original Research

# Development of a translational radiobiology platform using pancreatic cancer patient-derived organoids for personalized radiation oncology

Christopher Kessler [a,b], Francheska Cadacio [a], Carlo Maurer [c,d], Arlett Schäfer [c,d], Felix Orben [c], Julius C. Fischer [a], Daniela Schilling [a,e], Lisa Fricke [c,d], Sebastian Rasch [c], Ihsan E. Demir [f], Katja Steiger [b,g,h], Wilko Weichert [b,g,1], Roland M. Schmid [c], Stephanie E. Combs [a,b,e], Maximilian Reichert [b,c,d,i,2,*], Sophie Dobiasch [a,b,e,2,*]

[a] Department of Radiation Oncology, TUM School of Medicine and Health, TUM Klinikum Rechts der Isar, Technical University of Munich (TUM), Munich, Germany
[b] German Cancer Consortium (DKTK), Partner Site Munich, a partnership between DKFZ and University Hospital Klinikum rechts der Isar, Germany
[c] Medical Clinic and Polyclinic II, TUM School of Medicine and Health, TUM Klinikum Rechts der Isar, Technical University Munich (TUM), Munich, Germany
[d] Translational Pancreatic Cancer Research Center, Medical Clinic and Polyclinic II, TUM School of Medicine and Health, TUM Klinikum Rechts der Isar, Technical University of Munich (TUM), Munich, Germany
[e] Institute of Radiation Medicine (IRM), Helmholtz Zentrum München, Neuherberg, Germany
[f] Department of Surgery, TUM School of Medicine and Health, TUM Klinikum Rechts der Isar, Technical University of Munich (TUM), Munich, Germany
[g] Institute of Pathology, Technical University of Munich (TUM), Munich, Germany
[h] Comparative Experimental Pathology, Technical University of Munich (TUM), Munich, Germany
[i] Center for Organoid Systems (COS), Technical University of Munich (TUM), Garching, Germany

ARTICLE INFO

*Keywords:*
Pancreatic cancer
Patient-derived organoids
Personalized radiooncology
Radiobiological characterization
Translational research

ABSTRACT

Pancreatic ductal adenocarcinoma (PDAC) is one of the most aggressive malignancies with neoadjuvant radio (chemo)therapy failing in approximately 70 % of cases due to high tumor heterogeneity, and intrinsic radioresistance. Patient-derived organoids (PDOs) closely recapitulate appearance, and functionality as the original tissue and have potential to explore novel therapies for personalized radiooncology.

In this study, the radioresponse of PDAC PDO lines was determined after irradiation (RT). PDOs were immunohistochemically characterized by γ-H2AX, HIF-1α and Ki-67 staining. RNA sequencing data were analyzed by gene set enrichment analyses to investigate underlying mechanisms of radioresistance. Preclinical findings were correlated with clinical data from the corresponding patients.

PDOs showed a significant heterogeneity in response to radiation and were classified into radiosensitive, intermediate, and radioresistant subgroups. A correlation between radiosensitivity and enhanced proliferation and decreased hypoxia was observed. OXPHOS-related gene signatures were significantly overexpressed in the radioresistant phenotype. Translationally, radioresistance in PDOs was associated with significantly poorer survival of patients.

Our platform demonstrated heterogeneity in radioresponse reflecting the clinical situation and correlation with clinical outcomes. Immunohistochemical staining and transcriptomic profiling identified molecular signatures, including HIF-1α and OXPHOS-related pathways, associated with radioresistance. Implementing PDO-based radioresponse profiling in clinical workflows may enable patient stratified treatment approaches. Overall, our findings suggest that functionalizing PDOs for radioresponse might extend PDO-informed precision oncology.

* Corresponding authors.
*E-mail addresses:* maximilian.reichert@tum.de (M. Reichert), sophie.dobiasch@tum.de (S. Dobiasch).
[1] deceased in July 2023
[2] These authors contributed equally

https://doi.org/10.1016/j.tranon.2025.102535
Received 25 May 2025; Received in revised form 26 August 2025; Accepted 10 September 2025
Available online 17 September 2025

## Introduction

Pancreatic ductal adenocarcinoma (PDAC) is one of the most aggressive and lethal human malignancies. Its incidence is rising, and PDAC is projected to become the second leading cause of cancer-related death within the next decade. Despite intense efforts in basic research and the development of novel treatment strategies, the prognosis remains dismal, with a 5-year survival rate below 10 % [1]. The poor outcome is largely due to late diagnosis, high tumor heterogeneity, genetic variability, and a complex tumor microenvironment - factors that contribute to resistance to standard therapies such as radiotherapy (RT), chemotherapy (CT), and targeted agents [2,3]. To ensure optimal treatment, PDAC patients require multidisciplinary evaluation in tumor boards. Surgical resection remains the only curative option, yet only about 20 % of patients are diagnosed with a resectable tumor. Neoadjuvant treatments aim to downsize tumors and enable secondary resectability. The optimal therapeutic approach for patients with borderline or locally advanced PDAC remains still challenging. Clinical studies have shown a comparable outcome after successful downsizing to patients with a primary resectable disease [4,5]. According to current recommendations a FOLFIRINOX-based neoadjuvant CT has shown promising efficacy with a median overall survival (OS) of 24.2 months - superior to outcomes reported with gemcitabine in locally advanced PDAC [6]. The role of RT in PDAC is still debated. RT fails in about 70 % of all cases, and internationally standardized guidelines are lacking [7,8]. While some studies showed an effective downsizing [9,10], other trials failed to demonstrate a significant benefit of neoadjuvant RT [11,12].

Most preclinical models rely on conventional 2D cell lines cultured on plastic dishes due to ease of use, broad availability and minimal cost [13]. However, these models fail to reproduce the cellular complexity, architecture, function and physiological dynamics of human tumors [14], and mainly lack associated clinical data from patients [15]. In contrast, patient-derived organoids (PDOs) offer a promising novel 3-dimensional (3D) technology defined as groups of cells assembled in 3D structures with self-renewal and self-organization capacities, maintaining a similar appearance and functionality as the original tissue while preserving tumor genetics and heterogeneity [13]. Major advantages in comparison to 2D approaches are the recapitulation of the intra- and intertumoral heterogeneity, the preservation of tumor morphology and dynamic as well as the prediction of response to therapy in the clinic [16].

PDO-based RT platforms exist for several cancers, most notably colorectal cancer, where Hsu et al. demonstrated dose-response profiling, genetic radiosensitivity correlates, and clinical validation [17]. PDAC poses distinct challenges: profound radioresistance, dense hypoxic stroma, and marked interpatient heterogeneity shaping RT outcomes. With no predictive biomarkers and a controversial role of RT, a clinically annotated PDO-based platform for PDAC represents an unmet need to inform patient-specific RT decisions.

In this project, we employed a radiobiological platform using clinically annotated PDAC PDOs to characterize radiation response. Specifically, we analyzed radiation response and radiobiological features including DNA-damage, proliferation and hypoxia as well as differentially regulated gene expression signatures across a panel of PDO lines. In order to underscore the clinical relevance of our translational PDAC platform in radiation oncology, novel targets for radioresistance were revealed, and clinical data of the respective PDAC patients were correlated with experimental results.

## Materials and methods

### *Study approval*

This preclinical study was complemented by a retrospective analysis of clinical data. The collection and use of PDOs were approved by the ethics committee of the Technical University Munich (TUM) (protocol code 373/20 S-EB from 13 July 2020). Written informed consent was obtained from all patients prior to sample acquisition.

Clinical data was collected retrospectively using the clinical workstation system at the TUM Klinikum rechts der Isar.

### *Generation and cultivation of PDOs*

Tumor specimens were obtained either by endoscopic ultrasound-guided fine needle biopsy (Medical Clinic and Polyclinic II) or surgical resection (Department of Surgery) at TUM Klinikum rechts der Isar between 2019 and 2020. PDOs were generated in Patient-derived Organoid Unit within the Translational Pancreatic Cancer Research Center, Medical Clinic and Polyclinic II at TUM. Except one sample (B211) the PDOs were isolated from chemo-naïve tumor tissue. PDAC was diagnosed by a board-certified pathologist in all cases.

PDOs were generated and cultured following the protocol by Dantes et al. [16]. Tumor origin was confirmed by KRAS mutation status identified by Sanger-Sequencing [18]. PDOs were seeded in Matrigel (Basement Membrane Matrix Growth Factor Reduced, Corning) and cultured in special medium adapted from [19] based on DMEM/ F12 (1X, +*L*-Glutamine, +15 mM HEPES, 85 %vol, Gibco) supplemented with D-glucose (5 mg/ml), ITS + premix (0,5 %vol, Thermo Fisher Scientific), 3,3,5-Triiodo-L-Thyronine (5 nM, Sigma-Aldrich), dexamethasone (1 µM, Sigma-Aldrich), cholera toxin (100 ng/ml, Sigma-Aldrich), penicillin/streptomycin (1 %vol, Sigma-Aldrich), nu-serum IV (5 % vol, Thermo Fisher Scientific), murine EGF (20 ng/ml, PeproTech), bovine pituitary extract (25 µg/ml, Sigma-Aldrich), nicotinamide (10 mM, Sigma-Aldrich), A83–01 (0.5 µM, Stemcell Technologies), r-spondin conditioned medium (5 %vol, produced beforehand with 293t-HA-R-spo1-Fc cells according to manufacturer protocol, Trevigen), human heregulin β−1 (100 ng/ml, PeproTech) and 15.2 µMol/l Rho Kinase Inhibitor (Merck). PDOs were passaged every 1–2 weeks at a 1:2 ratio. Supernatants were routinely screened for mycoplasma using the MycoAlert Mycoplasma Detection Kit (Lonza) according to manufacturer`s protocol.

### *Irradiation*

Radiation was delivered at 200 kV and 15 mA with a dose rate of 0.90 Gy/min using the RS225A RT device (Gulmay/Xstrahl).

### *Cell viability assay and microscopic analysis after RT*

Response to RT was determined using the CellTiter-Glo (CTG) 3D Cell Viability Assay (Promega). PDOs were enzymatically dissociated with TrypLE (Express Enzyme 1x, Thermo Fisher Scientific) and seeded. After 24 h of incubation for organoid reassembly, cells were irradiated with 0, 2, 4, 6, or 8 Gy. Depending on the experiment, cells were incubated for an additional 72 h or one week followed by microscopic analysis and CTG viability assay. Brightfield microscopic images were obtained prior to cell lysis using Primovert microscope and Axiocam ERc 5 s (Carl Zeiss). Organoid area was measured in the software “QuPath” (The University of Edinburgh); for each condition, 15 representative organoids per each replicate were analyzed. CTG reagent was added at a 1:1 ratio. Plates were shaken for 10 min and incubated at room temperature for 20 min before luminescence was measured with a spectrophotometer (Varioskan LUX, Thermo-Fisher). Based on the radiation response at 8 Gy, PDOs were classified into three subgroups.

### *Immunohistochemistry*

For radiobiological characterization, PDOs were incubated for one week, and then irradiated with 0 Gy, 4 Gy or 8 Gy. PDOs were fixed 1 h after RT for γ-H2AX staining (Phospho-Histone H2A.X (Ser139) (20E3) Rabbit mAb, Cell Signaling Technology) and 24 h after RT for Ki-67

(Recombinant Anti-Ki67 antibody [SP6], Abcam) and HIF-1α (HIF-1α Antibody, Novus Biologicals). In addition, slices were stained for hematoxylin (Mayer's hematoxylin) and eosin (eosin y-solution 0.5 % aqueous) (HE). At the respective times PDOs were fixed in 4 % formalin for 2 h, transferred to 70 % ethanol, paraffin-embedded, and sectioned (2 μm). Immunohistochemistry (IHC) was performed using the automated BOND RX staining system (Leica Biosystems) according to the manufacturer's instruction. Slides were digitized using "Aperio AT2" slide scanner and analyzed quantitatively with "ImageScope" (Leica Biosystems) and "QuPath". For γ-H2AX and Ki-67, positive nuclei were quantified using the "positive cell detection" tool (based on optical density sum). HIF-1α-positive cells were identified by a manually trained multivariable random tree classifier.

### *Analysis of PDO gene expression data*

RNA-seq data were obtained from untreated PDOs, all processed within the same analysis batch. B169 was excluded due to batch variation, and no RNA-seq data were available for B326.

Genome-wide differential gene expression analysis was performed using the DESeq2 R package [20] on raw RNA-seq count data. A false discovery rate (FDR) $< 0.1$ was considered statistically significant. Phenotype-specific contrasts were defined based on radiosensitivity classification (sensitive, intermediate, resistant).

For gene set enrichment analysis (GSEA), class-specific gene expression signatures were generated by comparing each radiosensitivity group (e.g., resistant vs. rest) using DESeq2. These radiosensitivity-specific gene expression signatures (GES) were represented by Wald test statistics per gene and were interrogated by GSEA [21] using the HALLMARK gene set collection from MSigDb version 7.4 [22]. Results were visualized as normalized enrichment score (NES) heatmaps via the pheatmap R package.

For individual contrasts (e.g., resistant vs. sensitive), Wald statistic-based signatures were interrogated using both HALLMARK and PDAC subtype-specific gene sets (top 100 genes of basal-like and classical subtypes from Moffitt et al. [23]). NES values were computed using analytic rank-based enrichment analysis (aREA) [24], and enrichment/leading-edge results were visualized using custom Python scripts.

To identify transcriptomic correlates of radiosensitivity without predefined subgroups, genome-wide Pearson correlations were calculated between log2-transformed gene expression and 8 Gy post-irradiation viability (day 7). Positive correlations indicate higher expression in resistant PDOs, negative in sensitive ones. Empirical p-values were obtained from 10,000 permutations and cross-checked with subgroup-based differential expression (R v2025.05.1 + 513).

### *Correlation with clinical data*

Clinical data of the corresponding PDOs were collected retrospectively, including age at diagnosis, sex, tumor stage (UICC, Union for International Cancer Control), initial serum markers CA-19.9 and CEA, treatment (neoadjuvant/adjuvant CT, surgery), and outcome (distant metastasis-free survival (DMFS) and OS). Preclinical subgroups, defined by relative cell viability after 8 Gy RT, were compared and correlated with clinical parameters.

### *Statistics and reproducibility*

Cell viability assays were performed in $\geq 3$ independent experiments with 5 replicates per dose. Effects of RT on cell viability, PDO area and expression of the different IHC markers as well as on clinical data were analyzed using two-sided *t*-tests (unpaired for two groups).

Dose–response data were fitted with a linear-quadratic (LQ) model ($SF = \exp[-\alpha \cdot D - \beta \cdot D^2]$) normalized to non-irradiated controls (SF=1 at 0 Gy), with $\alpha \geq 0$ and $\beta \geq 0$. Model quality was assessed via $R^2$, AICc, and residuals. Curves were also fitted with the single-hit multi-target (SHMT) model [25] to derive $D_o$, n, and Dq (initial $D_o$=2 Gy, $n = 2$; $D_o > 0$, $n \geq 1$). Correlations used Pearson's R. Prognostic relevance for OS was evaluated with Cox regression (8 Gy viability, z-standardized), with proportional hazards assumptions tested via Schoenfeld residuals and model fit by Wald and likelihood ratio tests (R 2025.05.1 + 513).

For three-group comparisons, variance homogeneity was assessed with the Brown–Forsythe test; if violated ($p < 0.05$), Welch's ANOVA with Dunnett's T3 post-hoc test was applied, otherwise one-way ANOVA with Tukey's test. Dose-response data were fitted with a linear-quadratic (LQ) model (survival fraction (SF): $SF = \exp[-\alpha \times D - \beta \times D^2]$) normalized to non-irradiated controls (SF=1 at 0 Gy) with $\alpha \geq 0$ and $\beta \geq 0$. Model quality was assessed by $R^2$, corrected Akaike Information Criterion (AICc), and residuals. Curves were also fitted with the single-hit multi-target model (SHMT) [25] to derive $D_o$, n, and Dq (initial values $D_o$=2 Gy, $n = 2$; constraints $D_o > 0$, $n \geq 1$). Correlations used Pearson's.

Prognostic relevance for OS was evaluated with Cox regression (8 Gy viability, z-standardized) with proportional hazards assumptions tested with Schoenfeld residuals, and model fit by Wald and likelihood ratio tests (R 2025.05.1 + 513).

Analyses and plotting were performed using GraphPad Prism 9.5.1. (GraphPad Software, Inc). $P < 0.05$ was considered statistically significant.

## Results

### *Heterogeneity of radiation response*

To assess radioresponse in PDOs, viability assays and microscopic analysis were performed on a panel of nine PDO lines one week (Fig. 1A) and 72 h after RT (supplementary Fig. S1A). Growth behavior varied with increasing doses: higher RT doses led to smaller organoids, disrupted morphology, and loss of structural integrity (supplementary Fig. S2A). Relative cell viability at 8 Gy ranged from 0.31 (B283, ± 0.07) to 0.84 (B226, ± 0.17) after one week (Fig. 1B, supplementary Table S1).

Based on relative viability at 8 Gy one week after irradiation, PDO lines were stratified into radiosensitive (B283, B211, B326), intermediate (B169, B188, B290) and radioresistant (B320, B339, B226) groups. This classification was applied in an exploratory manner to contrast the most sensitive with the most resistant PDOs, while the intermediate group served as a transition category. Although viability values suggested a continuous distribution of radioresistance, this subgrouping facilitated the structured presentation of subsequent biological comparisons. LQ modelling yielded α/β parameters broadly consistent with the 8 Gy-based subgroups, particularly in resistant PDOs, but with overlaps between sensitive and intermediate lines. Poor fit quality and unstable β estimates supported 8 Gy viability as the more robust endpoint (supplementary Table S2).

Analysis with the SHMT model provided $D_o$, n, and Dq values (supplementary Table S2). Resistant PDOs showed high $D_o$ and in some cases broad shoulders, while sensitive PDOs had low $D_o$ and narrow shoulders. Intermediate lines again overlapped with sensitive PDOs, consistent with a continuum of radiosensitivity. However, low $R^2$ in several resistant PDOs highlighted the limited stability of SHMT fits in shallow survival curves.

Welch's ANOVA with Dunnett's T3 post-hoc test showed significant viability differences at 8 Gy between resistant and sensitive ($p \leq 0.01$) and resistant and intermediate PDOs ($p \leq 0.01$), but not between sensitive and intermediate ones ($p = 0.0913$; Fig. 1B, supplementary Fig. S2C). Mean organoid area at 8 Gy did not differ among groups (ANOVA $F(2,20)=1.185$, $p = 0.3263$; Fig. 1C, supplementary Fig. S2B), although a trend toward correlation with cell viability was observed ($p = 0.0686$, Pearson's $R = 0.6307$; Fig. 1D).

Taken together, our optimized experimental setup showed a significant heterogeneity in radioresponse with significant subgroup

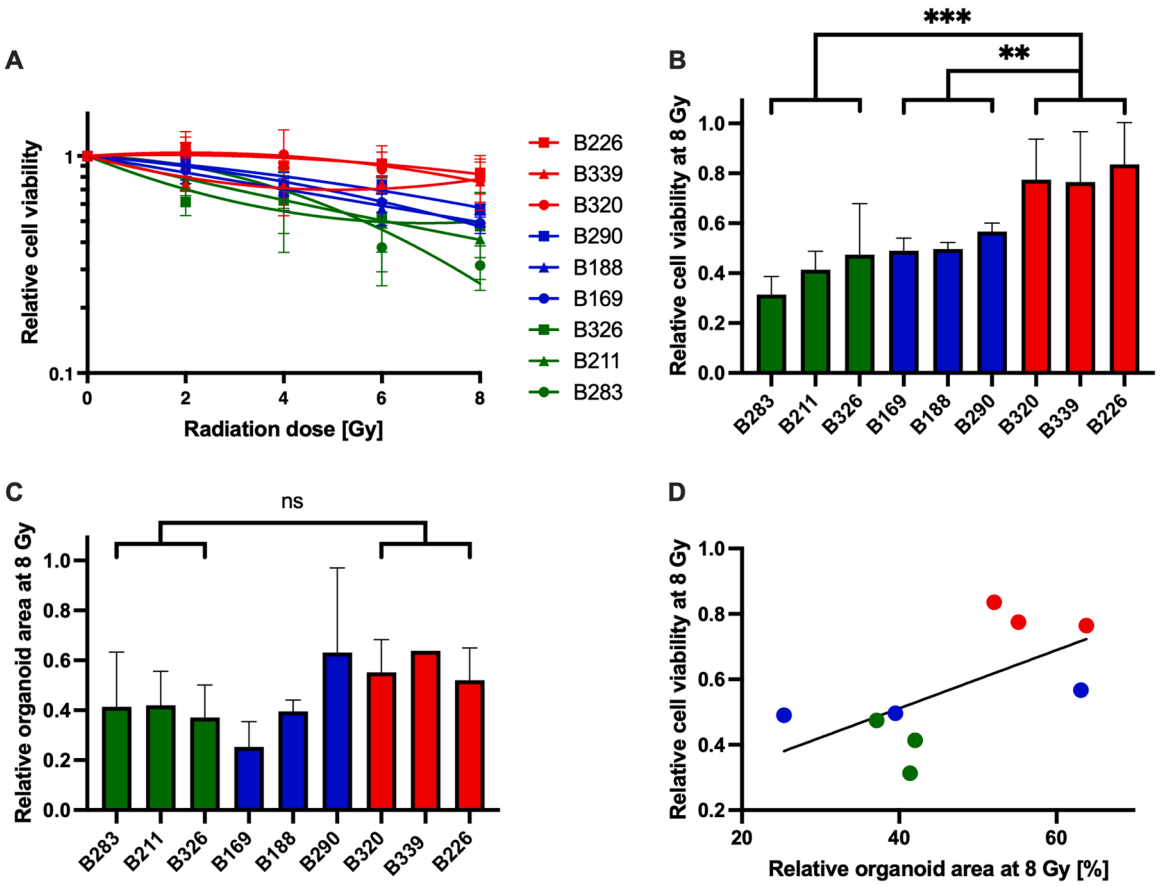


**Fig. 1.** Cell viability and organoid area (normalized to the respective 0 Gy control). Colors indicate radiosensitivity subgroups defined in the Results (green: radiosensitive, blue: intermediate, red: radioresistant). A) Relative cell viability of nine PDO lines, determined by CTG assay, one week after RT with 0, 2, 4, 6, and 8 Gy. Data represent at least three independent experiments. B) Comparison of the relative cell viability at 8 Gy across the nine PDO lines, grouped by radiosensitivity (sensitive, intermediate, resistant). Welch's ANOVA followed by Dunnett's T3 multiple comparisons test revealed significant differences between resistant vs. sensitive ($p = 0.0001$) and resistant vs. intermediate PDOs ($p = 0.0017$), but not between sensitive vs. intermediate PDOs ($p = 0.0924$; Supplementary Fig. S2C). C) Comparison of relative mean organoid area one week after 8 Gy RT. Ordinary one-way ANOVA (Brown–Forsythe $p = 0.8735$, indicating homogeneous variances) followed by Tukey's multiple comparisons test showed no significant differences among the three subgroups (ANOVA: $F(2,20) = 1.185$, $p = 0.3263$; pairwise comparisons: sensitive vs. intermediate $p = 0.9707$; sensitive vs. resistant $p = 0.3360$; intermediate vs. resistant $p = 0.4277$). D) Correlation between relative cell viability and mean organoid area at 8 Gy ($p = 0.0686$, Pearson's $R = 0.6307$).

differences in cell viability one week after RT in our panel of nine PDO lines but not in organoid area.

### *Radiobiological characterization by immunohistochemistry*

As surrogate of DNA damage, we determined baseline and radiation induced γ-H2AX staining (Fig. 2A2). No significant differences in baseline γ-H2AX levels were found among the three radiosensitivity subgroups (ANOVA $p = 0.82$). One hour after RT, the percentage of γ-H2AX positive cells (mean of all PDO cell lines) significantly increased from 0 Gy (38.6 %) to 4 Gy (87.7 %, $p \leq 0.0036$) and 8 Gy (89.5 %), $p \leq p = 0.0040$) with no further increase between 4 and 8 Gy. At 4 Gy, subgroup differences were not significant (ANOVA $p = 0.1421$). At 8 Gy, γ-H2AX levels differed significantly (ANOVA $p = 0.0013$), with radiosensitive PDOs showing higher staining than both intermediate (96.3 % vs. 85.5 %, $p = 0.0017$) and resistant lines (96.3 % vs. 86.7 %, $p = 0.0032$), while intermediate and resistant lines did not differ ($p = 0.7650$; Fig. 2A1).

Proliferative activity was evaluated by Ki-67 staining at baseline and 24 h after RT (Fig. 2B2). Radiosensitive PDOs exhibited significantly higher baseline Ki-67 expression compared to the combined intermediate/resistant groups (60.7 % vs. 34.7 %, $p \leq 0.0426$; Fig. 2B1), while no further subgroup differences or radiation-induced changes were observed at 24 h.

Hypoxia was analyzed by HIF-1α staining (Fig. 2C2), a marker that is upregulated in response to hypoxic conditions. Radiosensitive PDOs showed a trend toward lower baseline expression compared to resistant lines (8.4 % vs. 57.2 %, $p = 0.062$; Fig. 2C1), but no additional differences among subgroups were detected at baseline or after RT.

In summary, the IHC staining (subgroup-specific quantification in supplementary Table S3) revealed significant decreased DNA-damage one hour after RT, decreased baseline proliferation, and increased baseline hypoxia in radioresistant PDO lines - suggesting potential mechanisms of intrinsic radioresistance.

### *Gene expression signatures associated with radioresistance*

Unbiased correlation analysis of gene expression with radiosensitivity (8 Gy viability) showed strong concordance with the subgroup-based differential expression analysis, with consistent gene overlap and directionality (Fig. 3). To uncover relevant pathways associated with radioresistance and potential targets for therapeutic approaches, baseline RNA-seq data from radiosensitive (B283, B211), intermediate (B188, B290) and radioresistant (B320, B339, B226) PDOs were compared. GSEA of HALLMARK gene sets revealed distinct expression patterns between subgroups (supplementary Fig. S3).

The radiosensitive subgroup showed significant upregulation of the epithelial-mesenchymal transition (EMT) signature compared to both the resistant (NES:2.06, $p_{adj} = 1.07 * 10^{-5}$) and intermediate groups

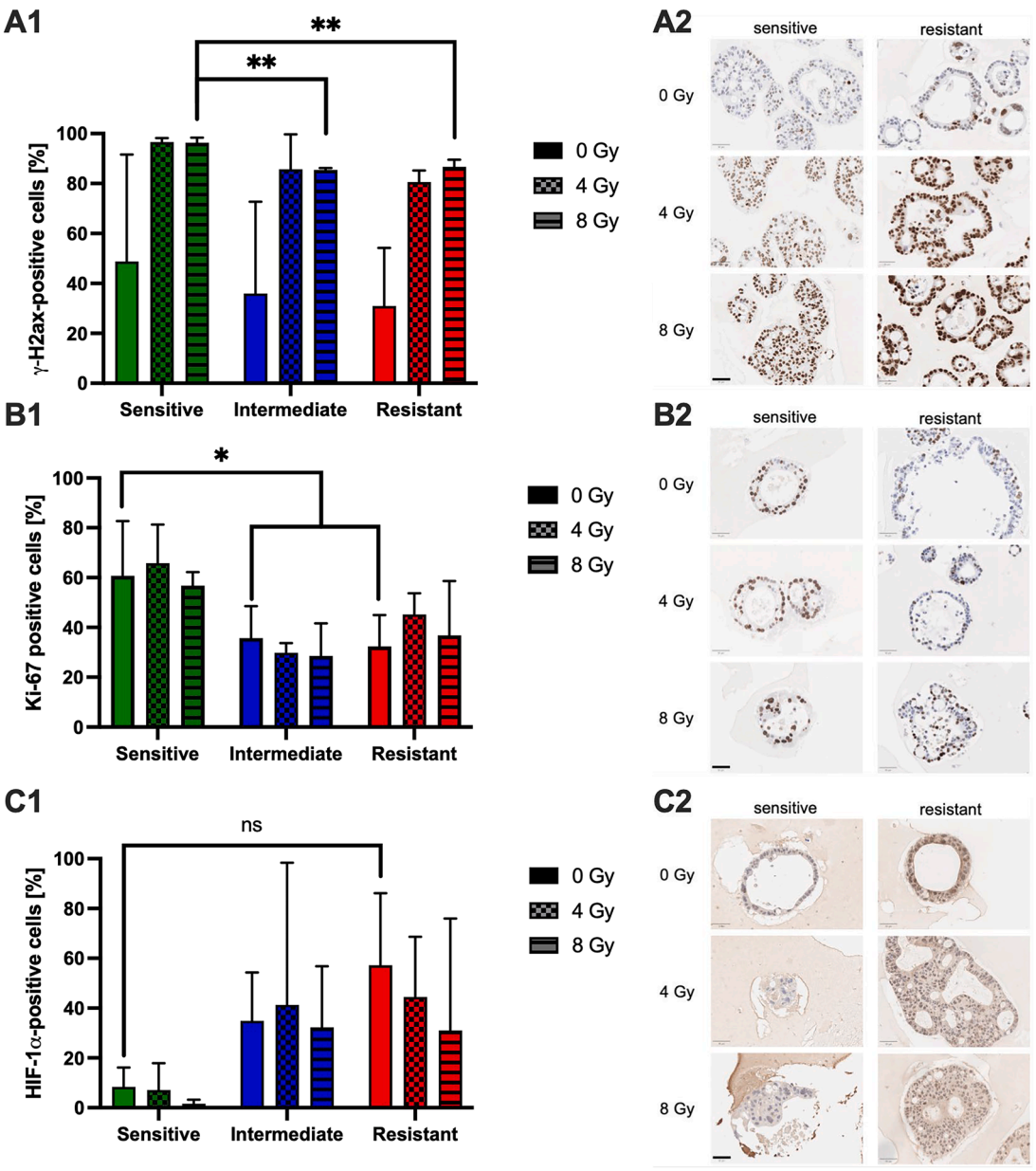


**Fig. 2.** Percentage of positive cells for γ-H2AX (A1, 1 h), Ki-67 (B1, 24 h), and HIF-1α (C1, 24 h) after RT with 0, 4, or 8 Gy in the sensitive (B283, B211, B326), intermediate (B169, B188, B290), and resistant (B320, B339, B226) subgroup. A1) γ-H2AX: No significant baseline differences were observed among the three subgroups (one-way ANOVA p = 0.82; Tukey's post-hoc: sensitive vs. intermediate p = 0.897; sensitive vs. resistant p = 0.814; intermediate vs. resistant p = 0.984). One hour after RT, γ-H2AX levels increased significantly (Brown–Forsythe p = 0.0003; Welch's ANOVA p = 0.0017). Dunnett's T3 post-hoc analysis confirmed significant increases from 0 Gy (38.6 %) to 4 Gy (87.7 %, p = 0.0036) and 8 Gy (89.5 %, p = 0.0040), with no difference between 4 Gy and 8 Gy (p = 0.95). At 4 Gy, subgroup differences were not significant (ANOVA p = 0.1421). At 8 Gy, ANOVA showed significant differences (p = 0.0013), with radiosensitive PDOs exhibiting higher γ-H2AX levels than intermediate (96.34 % vs. 85.46 %, p = 0.0017) and resistant lines (96.34 % vs. 86.68 %, p = 0.0032), while intermediate and resistant PDOs did not differ (p = 0.7650). B1) Ki-67: Radiosensitive PDOs showed significantly higher baseline expression compared to the combined intermediate and resistant groups (60.7 % vs. 34.7 %; F-test p = 0.2104; unpaired two-tailed *t*-test p = 0.0426). No further significant subgroup differences were observed, and no significant changes were detected 24 h after RT at 4 Gy or 8 Gy relative to baseline. C1) HIF-1α: Radiosensitive PDOs tended to have lower baseline expression than resistant lines (8.4 % vs. 57.2 %, p = 0.062), narrowly missing statistical significance. ANOVA revealed no significant differences among subgroups at baseline or 24 h post-irradiation with 4 Gy or 8 Gy. Representative IHC staining of γ-H2AX (A2: radiosensitive PDO B211; radioresistant PDO B226), Ki-67 (B2: radiosensitive PDO B326; radioresistant PDO B226), and HIF-1α (C2: radiosensitive PDO B211; radioresistant PDO B339). Scale bar = 50 μm.

(NES:2.09, $p_{adj} = 5.78 * 10^{-6}$), indicating reduced EMT activity in resistant and intermediate lines.

In contrast, the oxidative phosphorylation (OXPHOS) pathway was enriched in the radioresistant subgroup, suggesting enhanced mitochondrial respiration and oxygen-dependent metabolism (Fig. 4A) [26].

Further GSEA using PDAC subtype-specific gene sets [23] showed a strong association of the radioresistant subgroup with the "classical" subtype (NES: 6.47, $p_{adj} = 9.5 * 10^{-11}$), while the sensitive subgroup was linked to the more aggressive "basal-like" subtype (NES: 5.32, $p_{adj} = 1.1 * 10^{-7}$, Fig. 4B).

In summary, transcriptomic profiling identified subtype-specific expression differences, with OXPHOS activation and "classical" subtype enrichment as potential features of radioresistant PDOs and confirmed that these patterns are robust when radiosensitivity is treated as a continuous variable.

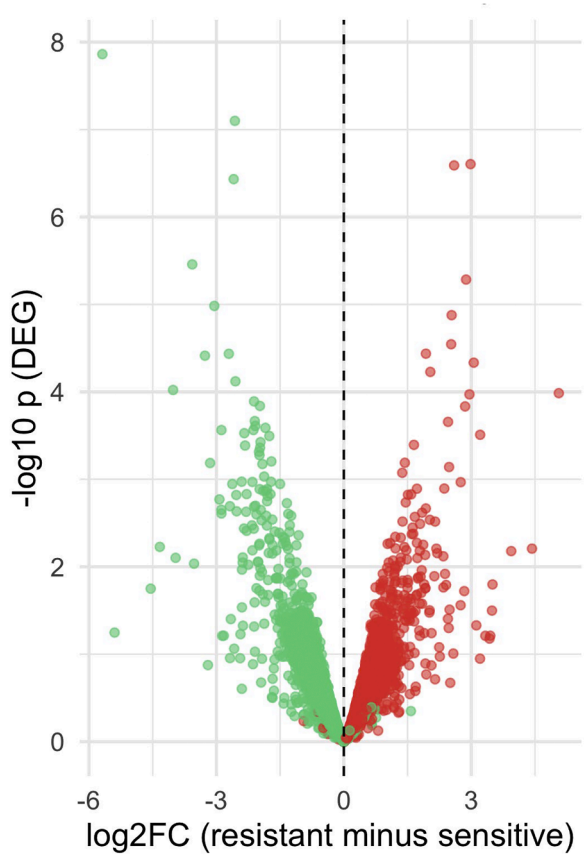


**Fig. 3.** Volcano plot of differentially expressed genes (DEGs) between radioresistant and radiosensitive PDO subgroups, colored according to their correlation with radiosensitivity (8 Gy post-irradiation viability). Each dot represents a single gene. The x-axis shows the $\log_2$ fold change (resistant minus sensitive), and the y-axis shows the $-\log_{10}$ p-value from the subgroup-based differential expression analysis. Genes positively correlated with viability (red) are predominantly upregulated in radioresistant PDOs, whereas genes negatively correlated (green) are upregulated in radiosensitive PDOs, confirming concordance between subgroup-based and correlation-based analyses.

*Explorative correlation of preclinical results with patient data for translational research*

To bridge gaps between the radiobiological characterization of PDOs and the clinical relevance of our translational PDO model, clinical data of the respective PDAC patients were correlated with our experimental data.

Patient characteristics including age at time point of diagnosis, sex, UICC tumor stage, baseline CA19–9 and CEA levels, treatment details, and outcomes (DMFS, OS), are summarized in Table 1. Mainly, all basic parameters were balanced within the three subgroups of radioresponse. Two PDO lines (B188 and B211) were derived from the same patient before (B188) and after (B211) neoadjuvant FOLFIRINOX treatment; B211 was excluded from clinical correlation as all other lines were derived from chemotherapy-naive tumors.

To assess prognostic value without predefined cut-offs, Cox regression was performed using 8 Gy viability as a continuous, z-standardized covariate. Higher viability was associated with increased hazard of death (HR per 1 SD = 4.92; 95 % CI 1.06–22.86; Wald $p = 0.042$; likelihood ratio $p = 0.013$), with proportional hazards assumption met (Schoenfeld $p = 0.18$). OS correlated strongly with *in vitro* viability at 8 Gy ($p = 0.0027$, Pearson's $R = -0.8943$, Fig. 5, Supplementary Table S4). Notably, the most radioresistant line (B226) was derived from the only patient with metastatic UICC stage IV disease, while the other resistant lines were from unresectable cases, consistent with poor prognosis.

Taken together, OS and clinical outcome was significantly worse in our radioresistant PDO subgroup, and radiosensitivity as a continuous measure remained an independent predictor, underscoring the translational value of our PDO model.

## Discussion

In this work, we established a preclinical setup to determine the radioresponse and the radiobiological characteristics of a PDO biobank. The response to RT in nine PDO-lines showed a high heterogeneity, and radiosensitive, intermediate and -resistant subgroups were identified, after optimizing the experimental design with the one-week time point after RT for readout. This offers the chance to integrate the *in vitro* radiosensitivity into the clinical decision making and personalized treatment.

PDAC PDOs provide the opportunity to evaluate new treatment options and to tailor the optimal personalized therapy for patients, as their genomic profile is equivalent to the individual patient's genomic

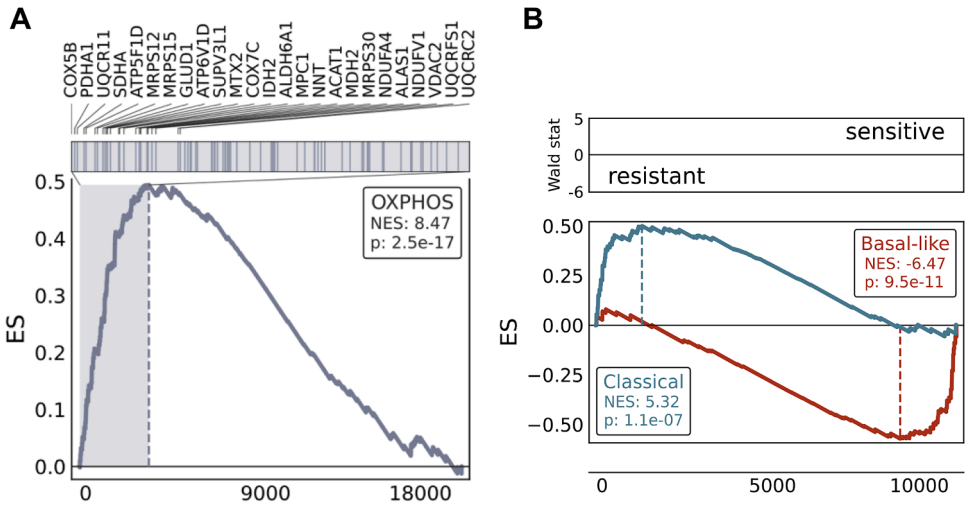


**Fig. 4.** A) GSEA of the radioresistant subgroup for OXPHOS dependent genes shows a significant upregulation of involved genes in comparison to the two other subgroups (NES 8.57, $p < 0.0001$). B) The radiosensitive subgroup is associated with "basal-like" and the radioresistant subgroup with "classical" subtype gene set by GSEA.

**Table 1**
Patient characteristics including age, sex, tumor stage, initial serum level of the tumor markers CA19–9 and CEA, treatment and clinical outcome.

| Preclinical subgroup | Relative viability at 8 Gy | PDO ID | Origin | Age [year] | Sex | UICC Stage | CA19–9 [U/ml] | CEA [ng/ml] | Neoadjuvant CT | Surgery | Adjuvant CT | DMFS [months] | OS [months] |
|---|---|---|---|---|---|---|---|---|---|---|---|---|---|
| Sensitive | 0.31 | B283 | endoscopy | 64 | m | III | 433 | 0.61 | FOLFIRINOX (sampling before) | 1 | mFOLFIRINOX | 42 | 42 |
| Sensitive | **0.41** | **B211** | surgery | 69 | m | III | 597 | 2.2 | FOLFIRINOX (sampling after) | 1 | FOLFIRINOX | 14 | 15 |
| Sensitive | 0.47 | B326 | surgery | 71 | w | III | 24 | 5.8 | NA | 1 | mFOLFIRINOX | 36 | 36 |
| intermediate | 0.49 | B169 | surgery | 78 | m | III | 2 | 7.6 | NA | 1 | Capecitabine | 43 | 43 |
| intermediate | **0.50** | **B188** | endoscopy | 69 | m | III | 597 | 2.2 | FOLFIRINOX (sampling before) | 1 | FOLFIRINOX | 14 | 15 |
| intermediate | 0.57 | B290 | surgery | 78 | w | III | 41 | 5.1 | NA | 1 | NA | 12 | 21 |
| Resistant | 0.77 | B320 | endoscopy | 80 | m | III | 313 | 6.28 | NA | 0 | NA | 1 | 1 |
| Resistant | 0.76 | B339 | surgery | 67 | m | III | 7 | 61.7 | NA | 1 | mFOLFIRINOX | 3 | 3 |
| Resistant | 0.84 | B226 | radiology | 61 | w | IV | 2 | 22.8 | Gemcitabine/ Paclitaxel | 0 | NA | 2 | 3 |

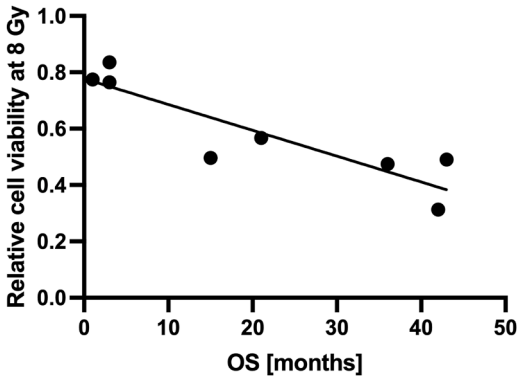


**Fig. 5.** Relationship between mean overall survival (OS) and *in vitro* radiosensitivity. Scatter plot of patient OS (months, x-axis) versus relative PDO cell viability at 8 Gy (y-axis; CTG assay, normalized to the untreated control), $n = 8$. Simple linear regression revealed a strong negative correlation (Pearson's $r = -0.8943$, $p = 0.0027$), indicating that higher *in vitro* viability, reflecting greater radioresistance, is associated with shorter OS.

heterogeneity [27]. Tiriac et al. demonstrated in comprehensive PDAC PDO library that the *in vitro* treatment response, as indicated by dose-response curves and the corresponding area under the curves, reflects the patient's response to CT. Additionally, the integration of DNA and RNA-seq allows for the development of individualized therapeutic approaches [28].

The use of PDAC PDOs to investigate the efficacy of RT is not well researched and implemented in the clinic yet compared to other tumor entities or treatment modalities.

Important first experiments evaluating the effects of RT in four different PDAC PDO lines were published by Naumann et al. [29]. In their study, cell viability following RT with different beam qualities (photons and protons) as well as combination treatments (RT with gemcitabine or 5-fluorouracil) was assessed using the PrestoBlue assay. Naumann et al. reported that viability differences observed at a dose of 6 Gy vanished 13 days post-RT compared to six days after RT [29]. In our experiments, we observed increasing heterogeneity in the radiation response between PDO lines at 8 Gy one week after RT compared to three days post-RT, suggesting divergent late responses. Naumann et al. also discussed limitations of the PrestoBlue assay, which primarily reflects metabolic activity and may fail to detect delayed radiation effects such as mitotic catastrophe, especially in slow-growing PDAC PDOs.

In contrast, our use of an ATP-based assay with a later readout (one-week post-RT) enabled more reliable detection of interline differences. This is consistent with the work of van Goor et al. using ATP-based assays in two PDAC PDO lines, which similarly concluded that extended observation periods are necessary to uncover relevant dose-response patterns [30].

Similarly, Yao et al. demonstrated that heterogeneity in cell viability persisted 15 days after RT in a cohort of 80 rectal cancer PDOs used to predict response to chemoradiation [31].

These findings underscore the importance of selecting appropriate time points and viability assays after RT to reliably capture biologically and clinically relevant differences.

The advantage and innovation of our current study lie in the broader screening of nine PDAC PDO lines, the additional in-depth radiobiological characterization including assessment of DNA damage, hypoxia, and proliferation by IHC, and most importantly the correlation of *in vitro* results with corresponding clinical patient data.

Radiosensitivity parameters from LQ and SHMT modelling broadly aligned with the 8 Gy-based classification at the extremes, but flat curves and unstable fits limited their utility in this small cohort. In contrast, 8 Gy viability was robust, measurable in all PDOs, and avoided uncertainties from extrapolation. The classification was applied exploratively to enable structured comparisons, with the intermediate category reducing misclassification near cutoffs and reflecting the continuous distribution of radiosensitivity.

To investigate radiobiological mechanisms, PDOs were stained for γ-H2AX, Ki-67, and HIF-1α at baseline and after RT. γ-H2AX staining reflected radiation-induced DNA double-strand breaks. Baseline differences were not significant, indicating that increases at 4 Gy and 8 Gy were irradiation-related. Radiosensitive PDOs showed significantly higher γ-H2AX levels after RT than resistant lines, consistent with greater DNA damage susceptibility and contributing to their higher radiosensitivity [32].

Ki-67 is a protein detectable in proliferating cells only [33], and a frequently used cellular marker to measure the portion of proliferating cells in a population and is gaining importance also in the prognosis of PDAC [34]. The radiosensitive PDO subgroup in our cohort has a significantly higher baseline percentage of Ki-67 positive cells, suggesting that high intrinsic proliferative activity may be linked to increased radiosensitivity, as reported for other tumor entities like rectal cancer [35], oral squamous cell carcinoma [36] and small cell lung cancer [37]. Our results support that Ki-67 might be used as prognostic marker for radiosensitivity in PDAC.

In contrast, no consistent changes in Ki-67 were observed 24 h after irradiation in any subgroup, suggesting either absence of immediate proliferative arrest or that effects such as mitotic catastrophe occur later. Additional time points beyond 24 h could help to clarify the temporal dynamics of proliferation after RT, but were outside the scope of the

present study and should be addressed in future work. Nevertheless, these findings support the potential of Ki-67 as a prognostic marker for radiosensitivity in PDAC.

HIF-1α is a subunit of a transcription factor, which is upregulated among other reasons as a response to hypoxia [38]. Elevated HIF-1α is associated with worse prognosis, earlier occurring of metastasis and radioresistance in PDAC [39,40]. In our cohort, radiosensitive PDOs showed a trend toward lower HIF-1α expression. This supports its potential as a predictive marker and therapeutic target for radiosensitization.

We assume that by combining these three markers (γ-H2AX, Ki-67 and HIF-1α), IHC could provide a strong tool for the radiobiological characterization and prediction of radioresponse.

In our work, the comparison of the two PDO lines B188 and B211 is of particular note, because these specimens are derived from the same patient before (B188) and after (B211) neoadjuvant treatment with FOLFIRINOX. Our results showed an increased response to RT of B211 compared to B188. As an induction CT has the potential to change the genetic profile of tumors, RT might be a promising second therapeutic option for locally advanced PDAC as recommended in international guidelines. These results require confirmation by further pairs of PDOs generated before and after CT.

The rapid availability of the RNA-seq data enables fast decision-making in the clinical routine in the best interest of the patient.

OXPHOS is beside glycolysis the cells main source of ATP. OXPHOS is carried out in the mitochondria, with the need of oxygen as terminal electron acceptor. Despite hypoxic conditions in many cancer entities, the upregulation of glycolysis to comply with the extensive need for energy (Warburg-effect) is not accompanied with a downregulation of OXPHOS [41]. It was demonstrated, that a resistant subpopulation is highly dependent on OXPHOS for survival and can sufficiently be addressed with OXPHOS inhibitors (oligomycin) in a PDAC mouse model [42]. Our results show a significant upregulation of OXPHOS in the radioresistant subgroup using GSEA. Targeting this pathway might be a promising approach to sensitize particularly radioresistant PDAC by increasing tumor oxygen levels and to overcome radioresistance [43].

Transcriptomic differences between radiosensitive and radioresistant PDOs remained consistent when radiosensitivity was analyzed as a continuous variable, supporting their robustness and indicating genuine biological rather than classification-derived effects.

The prospective COMPASS trial demonstrated the feasibility of predictive mutational signatures in advanced PDAC, showing better response to mFOLFIRINOX in patients with the “classical” than the “basal-like” subtype [44]. To date, no data exist on subtype-specific radiotherapy response. We therefore analyzed our PDOs by GSEA and found that radiosensitive lines predominantly exhibited a “basal-like” and resistant lines a “classical” signature, suggesting that RT might benefit aggressive, chemo-resistant tumors. Supporting this, An et al. reported higher sensitivity of “basal-like” PDOs to Metavert, a dual GSK3-β/HDAC inhibitor, compared to irinotecan-based chemotherapy [45].

Hsu et al. demonstrated in rectal cancer that PDOs can predict radiosensitivity by integrating mutational profiling, dose-response modeling, and mechanistic assays with clinical outcomes [17]. Our study extends this PDO-based approach to PDAC, highlighting its applicability in a tumor type with pronounced radioresistance, dense stroma, and marked interpatient heterogeneity, and addressing the unique challenges that distinguish PDAC from rectal cancer. Treating radiosensitivity as a continuous variable in a Cox model confirmed its significant association with OS, independent of subgroup cut-offs. This underscores the robustness of the relationship and the prognostic potential of PDO-based radiosensitivity.

Furthermore, the only primary metastasized UICC tumor stage IV as well as unresectable diseases were observed in the radioresistant subgroup. The other parameters like age at diagnosis, sex or initial level of common tumor markers CA19–9 and CEA did not show any correlation with the preclinical results. Although the data set is rather small, we demonstrated a trend towards worse survival and clinically more aggressiveness in the radioresistant subgroup.

Limitations of our study arise from the small sample size as well as from the clinical heterogeneity regarding specimen origin, and treatment.

Another limiting factor is the missing of stromal components in the TME of the PDOs. PDAC is known to feature an intratumoral heterogeneity on transcriptional level in different areas of the primary side [46]. As PDOs are derived from mostly only one location in the tumor, this also limits the translation of the *in vitro* results to the patient, but which could be overcome in the future with multiple samples.

To our knowledge, we were the first to develop a PDAC PDO-based platform to investigate the response to RT as well as the radiobiological characteristics and the correlation of preclinical with corresponding clinical data for implementation of real translational research.

## Conclusion

Our translational platform using PDAC PDOs enabled characterization of the radiation response, identification of radiobiological features, and detection of radioresistance patterns, suggesting a predictive potential for personalized therapeutic approaches in radiation oncology. The high heterogeneity among PDOs in response to RT reflect the clinical situation. We gained insights into key mechanisms of radioresistance and revealed hypoxia as a potential driver of radioresistance in our cohort. Moreover, OXPHOS pathway activation emerged as a promising target for radiosensitization. Notably, *in vitro* radioresistance correlated with poor clinical outcomes, highlighting the clinical relevance of our PDO model. Prospectively, we aim to implement PDO-based radiosensitivity screening in clinical workflows to enable truly personalized RT in PDAC patients.

## Glossary

Akaike information criterion (AICc); analytic rank-based enrichment analysis (aREA); chemotherapy (CT); CellTiter-Glo (CTG); 3-dimensional (3D); distant metastases-free survival (DMFS); DNA-double strand break (DSB); epithelial-mesenchymal transition (EMT); false discovery rate (FDR); gene set enrichment analysis (GSEA); hematoxylin and eosin (HE); immunohistochemistry (IHC); linear-quadratic (LQ); normalized enrichment score (NES); overall survival (OS); oxidative phosphorylation (OXPHOS); pancreatic ductal adenocarcinoma (PDAC); patient-derived organoids (PDOs); radiotherapy (RT); single-hit multi-target model (SHMT); survival fraction (SF); UICC (Union for International Cancer Control).

## Funding sources

This work was supported in part by the Deutsche Forschungsgemeinschaft (DFG, German Research Foundation) – project number 329628492 - SFB 1321 Project P15, and Project S01. M.R. acknowledges the financial support by the German Cancer Aid (Max-Eder Program 111273 and 70114328) and the German Research Foundation (DFG, SFB1321 Modeling and Targeting Pancreatic Cancer, Projects S01 and TP12, Project ID329628492 and Project RE 3723/4–1). J.C.F was supported by the Else-Kröner-Fresenius-Stiftung (2022_EKMS.26). M.R. was supported by the DKTK (German Consortium for Translational Cancer Research) Strategic Initiative Organoid Platform.

## Ethics in publishing

The work described has been carried out in accordance with The Code of Ethics of the World Medical Association (Declaration of Helsinki) for experiments involving humans.

## CRediT authorship contribution statement

**Christopher Kessler:** Writing – original draft, Visualization, Methodology, Investigation, Formal analysis. **Francheska Cadacio:** Methodology, Investigation. **Carlo Maurer:** Formal analysis. **Arlett Schäfer:** Methodology. **Felix Orben:** Methodology. **Julius C. Fischer:** Writing – review & editing, Visualization. **Daniela Schilling:** Writing – review & editing, Visualization. **Lisa Fricke:** Methodology. **Sebastian Rasch:** Methodology. **Ihsan E. Demir:** Methodology. **Katja Steiger:** Methodology, Formal analysis. **Wilko Weichert:** Methodology. **Roland M. Schmid:** Supervision, Resources. **Stephanie E. Combs:** Writing – review & editing, Supervision, Resources, Conceptualization. **Maximilian Reichert:** Writing – review & editing, Project administration, Methodology, Conceptualization. **Sophie Dobiasch:** Writing – original draft, Validation, Project administration, Methodology, Investigation, Conceptualization.

## Declaration of competing interest

none.

## Acknowledgments

We thank Olga Seelbach, Marion Mielke, and Marlon Stein for excellent technical support. C.K. was supported by the structured graduation program “Translational Medicine” (Else Kröner Graduate School) of TUM. S.D. acknowledges “Hans und Klementia Langmatz Stiftung”, the KKF, Medical Faculty of the Technical University of Munich (TUM) and “Translational & Clinical Projects”, Helmholtz Zentrum München (G-508200–035) for research support.

## Supplementary materials

Supplementary material associated with this article can be found, in the online version, at doi:10.1016/j.tranon.2025.102535.

## References

[1] W. Park, A. Chawla, E.M. O'Reilly, A review of pancreatic cancer-reply, JAMA 326 (23) (2021) 2436–2437.
[2] K. Feldmann, et al., Mesenchymal plasticity regulated by Prrx1 drives aggressive pancreatic cancer biology, Gastroenterology (2020).
[3] S. Mueller, et al., Evolutionary routes and KRAS dosage define pancreatic cancer phenotypes, Nature 554 (7690) (2018) 62–68.
[4] D. Habermehl, et al., Neoadjuvant chemoradiation with Gemcitabine for locally advanced pancreatic cancer, Radiat. Oncol. 7 (2012) 28.
[5] O. Simon, et al., Pancreatic cancer in the year 2018 - room for Precision medicine?], Dtsch. Med. Wochenschr. 143 (15) (2018) 1109–1112.
[6] M. Suker, et al., *FOLFIRINOX for locally advanced pancreatic cancer: a systematic review and patient-level meta-analysis*, Lancet Oncol 17 (6) (2016) 801–810.
[7] S. Dobiasch, et al., Essential role of radiation therapy for the treatment of pancreatic cancer: novel study concepts and established treatment recommendations, Strahlenther. Onkol. 194 (3) (2018) 185–195.
[8] M. Orth, et al., Pancreatic ductal adenocarcinoma: biological hallmarks, current status, and future perspectives of combined modality treatment approaches, Radiat. Oncol. 14 (1) (2019) 141.
[9] A.G. Morganti, et al., A systematic review of resectability and survival after concurrent chemoradiation in primarily unresectable pancreatic cancer, Ann. Surg. Oncol. 17 (1) (2010) 194–205.
[10] E. Versteijne, et al., *Neoadjuvant chemoradiotherapy* versus *upfront surgery for resectable and borderline resectable pancreatic cancer: long-term results of the Dutch randomized PREOPANC trial*, J. Clin. Oncol. (2022) Jco2102233.
[11] V. Festa, et al., Neoadjuvant chemo-radiotherapy for patients with borderline resectable pancreatic cancer: a meta-analytical evaluation of prospective studies, JOP 14 (6) (2013) 618–625.
[12] P. Hammel, et al., *Effect of chemoradiotherapy* vs *chemotherapy on survival in patients with locally advanced pancreatic cancer controlled after 4 months of Gemcitabine with or without Erlotinib: the LAP07 randomized clinical trial*, JAMA 315 (17) (2016) 1844–1853.
[13] L. Moreira, et al., Pancreas 3D organoids: current and future aspects as a research platform for personalized medicine in pancreatic cancer, Cell Mol. Gastroenterol. Hepatol. 5 (3) (2018) 289–298.
[14] M. Fujii, T. Sato, Somatic cell-derived organoids as prototypes of human epithelial tissues and diseases, Nat. Mater. 20 (2) (2021) 156–169.
[15] N. Palechor-Ceron, et al., Conditional reprogramming for patient-derived cancer models and next-generation living biobanks, Cells 8 (11) (2019).
[16] Z. Dantes, et al., Implementing cell-free DNA of pancreatic cancer patient-derived organoids for personalized oncology, JCI Insight 5 (15) (2020).
[17] K.S. Hsu, et al., Colorectal cancer develops inherent radiosensitivity that can Be predicted using patient-derived organoids, Cancer Res. 82 (12) (2022) 2298–2312.
[18] F. Orben, et al., Epigenetic drug screening defines a PRMT5 inhibitor–sensitive pancreatic cancer subtype, JCI Insight 7 (10) (2022).
[19] K. Peschke, et al., Identification of treatment-induced vulnerabilities in pancreatic cancer patients using functional model systems, EMBO Mol. Med. 14 (4) (2022) e14876.
[20] M.I. Love, W. Huber, S. Anders, Moderated estimation of fold change and dispersion for RNA-seq data with DESeq2, Genome. Biol. 15 (12) (2014) 550.
[21] A. Subramanian, et al., Gene set enrichment analysis: a knowledge-based approach for interpreting genome-wide expression profiles, Proc. Natl. Acad. Sci. U S A 102 (43) (2005) 15545–15550.
[22] A. Liberzon, et al., The Molecular Signatures Database (MSigDB) hallmark gene set collection, Cell Syst. 1 (6) (2015) 417–425.
[23] R.A. Moffitt, et al., Virtual microdissection identifies distinct tumor- and stroma-specific subtypes of pancreatic ductal adenocarcinoma, Nat. Genet. 47 (10) (2015) 1168–1178.
[24] M.J. Alvarez, et al., Functional characterization of somatic mutations in cancer using network-based inference of protein activity, Nat. Genet. 48 (8) (2016) 838–847.
[25] M.L. Martin, et al., Organoids reveal that inherent radiosensitivity of small and large intestinal stem cells determines organ sensitivity, Cancer Res. 80 (5) (2020) 1219–1227.
[26] G. Reyes-Castellanos, R. Masoud, A. Carrier, Mitochondrial metabolism in PDAC: from better knowledge to new targeting strategies, Biomedicines 8 (8) (2020).
[27] I. Romero-Calvo, et al., Human organoids share structural and genetic features with primary pancreatic adenocarcinoma tumors, Mol. Cancer Res. 17 (1) (2019) 70–83.
[28] H. Tiriac, et al., Organoid profiling identifies common responders to chemotherapy in pancreatic cancer, Cancer Discov. 8 (9) (2018) 1112–1129.
[29] M. Naumann, et al., Combined systemic drug treatment with proton therapy: investigations on patient-derived organoids, Cancers 14 (15) (2022).
[30] I. van Goor, et al., Radiation response assessment of organoids derived from patients with pancreatic cancer, Clin. Transl. Radiat. Oncol. 48 (2024) 100829.
[31] Y. Yao, et al., Patient-derived organoids predict chemoradiation responses of locally advanced rectal cancer, Cell Stem. Cell 26 (1) (2020) 17–26, e6.
[32] E.P. Rogakou, et al., DNA double-stranded breaks induce histone H2AX phosphorylation on serine 139, J. Biol. Chem. 273 (10) (1998) 5858–5868.
[33] J. Gerdes, et al., Cell cycle analysis of a cell proliferation-associated human nuclear antigen defined by the monoclonal antibody Ki-67, J. Immunol. 133 (4) (1984) 1710–1715.
[34] I. Pergolini, et al., Prognostic impact of ki-67 proliferative index in resectable pancreatic ductal adenocarcinoma, BJS Open 3 (5) (2019) 646–655.
[35] C. Rödel, et al., Apoptosis as a cellular predictor for histopathologic response to neoadjuvant radiochemotherapy in patients with rectal cancer, Int. J. Radiat. Oncol. Biol. Phys 52 (2) (2002) 294–303.
[36] C. Freudlsperger, et al., Ki-67 expression predicts radiosensitivity in oral squamous cell carcinoma, Int. J. Oral Maxillofac. Surg. 41 (8) (2012) 965–969.
[37] N. Ishibashi, et al., Correlation between the Ki-67 proliferation index and response to radiation therapy in small cell lung cancer, Radiat. Oncol. 12 (1) (2017) 16.
[38] N. Elzakra, Y. Kim, HIF-1α metabolic pathways in Human cancer, Adv. Exp. Med. Biol. 1280 (2021) 243–260.
[39] A. Zoa, et al., High expression of hypoxia-inducible factor 1-alpha predicts poor prognosis in pancreatic ductal adenocarcinoma: a meta-analysis and database validation protocol, Transl. Cancer Res. 11 (9) (2022) 3080–3091.
[40] Y. Xia, L. Jiang, T. Zhong, The role of HIF-1α in chemo-/radioresistant tumors, OncoTargets Ther. 11 (2018) 3003–3011.
[41] T.M. Ashton, et al., Oxidative phosphorylation as an emerging target in cancer therapy, Clin. Cancer Res. 24 (11) (2018) 2482–2490.
[42] A. Viale, et al., Oncogene ablation-resistant pancreatic cancer cells depend on mitochondrial function, Nature 514 (7524) (2014) 628–632.
[43] G.S. Higgins, et al., Drug radiotherapy combinations: review of previous failures and reasons for future optimism, Cancer Treat. Rev. 41 (2) (2015) 105–113.
[44] K.L. Aung, et al., Genomics-driven precision medicine for advanced pancreatic cancer: early results from the COMPASS trial, Clin. Cancer Res. 24 (6) (2018) 1344–1354.
[45] J. An, et al., Metavert synergises with standard cytotoxics in human PDAC organoids and is associated with transcriptomic signatures of therapeutic response, Transl. Oncol. 49 (2024) 102109.
[46] X. Liu, et al., Multi-omics analysis of intra-tumoural and inter-tumoural heterogeneity in pancreatic ductal adenocarcinoma, Clin. Transl. Med. 12 (1) (2022) e670.